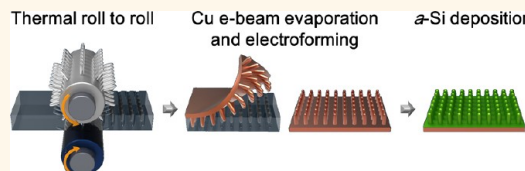


# 3D Amorphous Silicon on Nanopillar Copper Electrodes as Anodes for High-Rate Lithium-Ion Batteries

Gyutae Kim,<sup>†,§</sup> Sookyung Jeong,<sup>‡,§</sup> Ju-Hyeon Shin,<sup>†</sup> Jaephil Cho,<sup>‡,\*</sup> and Heon Lee<sup>†,\*</sup>

<sup>†</sup>Department of Materials Science and Engineering, Korea University, Seongbuk-gu, Anam-ro 145, Seoul, Republic of Korea, and <sup>‡</sup>Interdisciplinary School of Green Energy, Ulsan National Institute of Science and Technology (UNIST), 689-798, Ulsan, Republic of Korea. <sup>§</sup>G. Kim and S. Jeong contributed equally to this work.

**ABSTRACT** We present an amorphous Si anode deposited on a Cu nanopillar current collector, fabricated using a thermal roll-to-roll process followed by electroformation and LPCVD, for application in high-rate Li-ion batteries. Cu nanopillar current collectors with diameters of 250 and 500 nm were patterned periodically with 1  $\mu$ m pitch and 2  $\mu$ m height to optimize the diameters of the pillars for better electrochemical performance. Void spaces between Cu nanopillars allowed not only greater effective control of the strain caused by the Si expansion during lithiation than that allowed by a nonpatterned electrode but also significantly improved cycle performance even at 20 C measured after the same rate test: After 100 cycles at 0.5 C, the patterned electrodes with 250 and 500 nm diameter nanopillars showed high capacity retentions of 86% and 84%, respectively. These electrodes retained discharge capacities of 1057 and 780 mAh/g even at 20 C, respectively.



**KEYWORDS:** patterned current collector · thin-film Si · roll to roll · Li-ion battery · high C rate

On the recent development of electronic devices such as personal computers and smart phones, wearable devices have become remarkably attractive as the next generation of smart devices, heralding a paradigm shift in trends from portable to wearable devices. Because wearable devices need to be more compact and lightweight and need to retain the high performance of portable ones, Li-ion batteries play a key role in this paradigm shift. Thin-film batteries are the most suited for this application and provide a major breakthrough in the size reduction of wearable devices while maintaining high energy density.<sup>1–5</sup> However, the use of carbon-based materials in a conventional system does not meet the demands owing to their low theoretical capacity (372 mAh/g).<sup>6</sup>

Among the various potential anode materials, Si has been intensively investigated because it imparts a high theoretical capacity to the electrodes (4200 mAh/g) that is over 10 times higher than that of graphite.<sup>7</sup> Despite these superior characteristics, Si undergoes a 400% change in volume during lithiation, which results in pulverization and degradation of the electrical connection between electrodes.<sup>8–11</sup> This disadvantage is the main factor in the significant capacity

loss in the system during the electrochemical reaction (*i.e.*,  $\text{Si} + x\text{Li}^+ + xe^- \leftrightarrow \text{Li}_x\text{Si}$ ).<sup>12</sup> To prevent this crack formation caused by the stress in Si during cycling, two basic principles are applied in nanoengineering of Si-based electrodes to reduce the strain as follows:<sup>13–23</sup> (i) Empty space is incorporated into the electrode for effective accommodation of strain during cycling. There have been reports that Si nanowires,<sup>13</sup> Si nanotubes,<sup>20</sup> and Si nanoparticles encapsulated in hollow carbon tubes<sup>24</sup> are used for nanoengineered active materials;<sup>25–29</sup> (ii) Si thin film that is thinner than the critical thickness is deposited on the planar surface of the current collector using various deposition processes to prevent the loss of electrical connectivity between the active materials and the current collector.<sup>30–32</sup>

With respect to the two approaches, three-dimensional (3D) nanostructured electrodes have been widely considered because they significantly improve Li-ion diffusion and electron transport to overcome the low energy per unit area limitation of planar electrodes.<sup>33–36</sup>

Accordingly, we demonstrate a 3D nanostructured thin-film electrode consisting of Cu nanopillars fabricated using roll-to-roll hot embossing followed by Cu electroforming

\*Address correspondence to  
(J. Cho) [jpcho@unist.ac.kr](mailto:jpcho@unist.ac.kr);  
(H. Lee) [heonlee@korea.ac.kr](mailto:heonlee@korea.ac.kr).

Received for review December 17, 2013  
and accepted January 21, 2014.

Published online January 21, 2014  
10.1021/nn406464c

© 2014 American Chemical Society

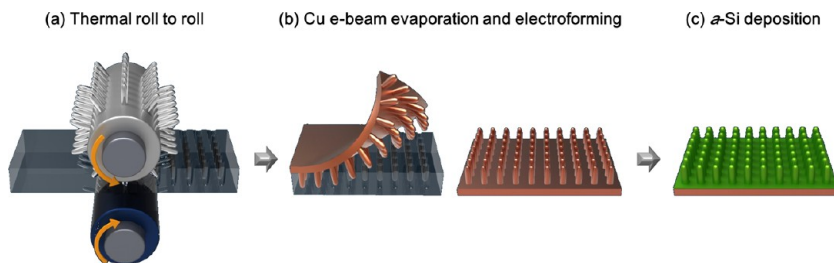


**Figure 1.** Schematic of the fabrication of 3D amorphous Si on a Cu nanopillar electrode. (a) Patterned polyvinyl chloride obtained from thermal roll-to-roll processing, (b) Cu nanopillar substrate applied *via* electroplating, (c) amorphous Si deposited on the Cu nanopillar substrate by low-pressure chemical vapor deposition.

with the  $\alpha$ -Si thin layer coated on Cu nanopillars *via* low-pressure chemical vapor deposition (LPCVD). As a current collector, a Cu nanopillar substrate provides a high surface area for better mass accommodation of Si deposition, while the space between Cu nanopillars enhances the electrochemical reaction between the electrode and electrolyte and accommodates the volume change during cycling. In addition, because the fabrication of the Cu nanopillar substrate involves only conventional top-down processes, the nanopillars can be generated through a facile and fast process with control of the surface area and simple modulation of the nanopillar density or diameter. Remarkably, the well-patterned nanopillar substrate imparts a significantly enhanced connection between the current collector and active materials without a binder and also provides free space to accommodate Si expansion without pulverization during cycling.

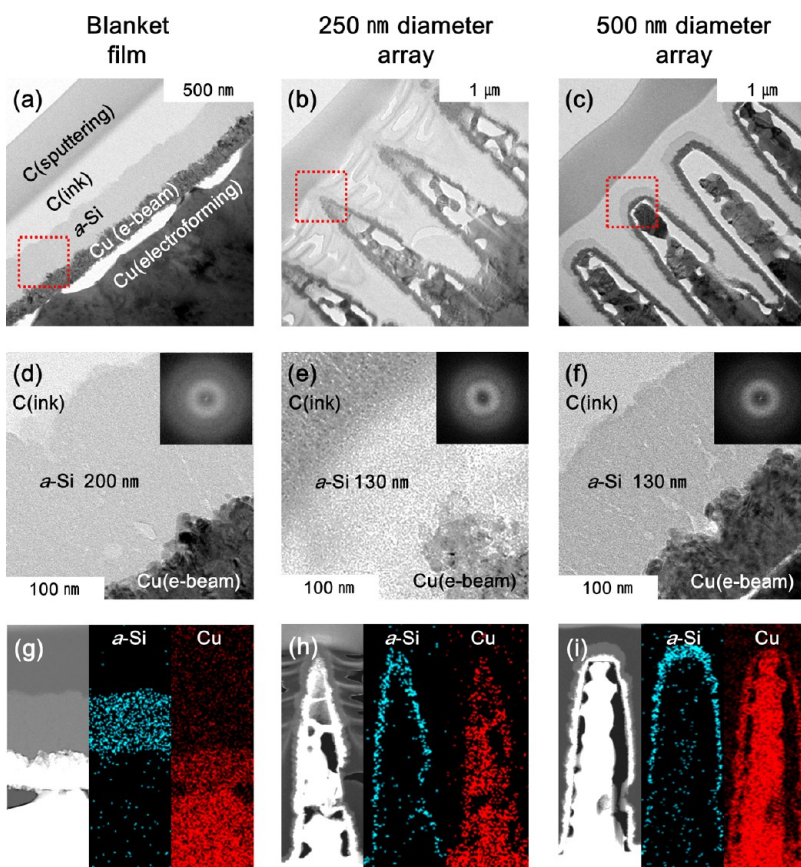
## RESULTS AND DISCUSSION

Figure 1 shows a schematic of the fabrication of the electrode comprising amorphous Si deposited on a 3D Cu nanopillar substrate ( $\alpha$ -Si/3D-Cu nanopillar electrode). First, Ni metal plate stamps with pitches of  $1\ \mu\text{m}$ , heights of  $2\ \mu\text{m}$ , and diameters of either 250 or 500 nm were fabricated. In the fabrication process of a Ni stamp, the height of  $2\ \mu\text{m}$  was the optimal dimension to reproduce the desired pattern by the thermal roll-to-roll method. If the aspect ratio of the pillar is too high ( $>9$ ) in our experimental conditions, the Ni pillars were deformed during contact with the PVC film, as shown in Figure S1. Then, the prepared patterned Ni stamp was transferred to polyvinyl chloride (PVC, glass transition temperature =  $80\ ^\circ\text{C}$ ) at  $100\ ^\circ\text{C}$  and  $\sim 10\ \text{atm}$  to prepare the patterned mold (Figure 1a). The Cu nanopillar substrate was formed by deposition of Cu onto the embossed PVC mold by e-beam evaporation at  $60\ ^\circ\text{C}$  and  $2.7 \times 10^{-5}\ \text{atm}$  to form a seed layer by 100 nm followed by electroformation at  $0.02\ \text{A}$  for 1 h in a Cu plating solution ( $\text{CuSO}_4 \cdot 5\text{H}_2\text{O}/\text{H}_2\text{SO}_4 = 2.5:1$  with 70 ppm HCl) (Figure 1b). Finally, the well-arrayed Cu nanopillar substrate (Figure S2) was detached from the polymer mold, and amorphous Si was deposited onto the prepared substrate by LPCVD using 2%  $\text{SiH}_4$  at  $200\ ^\circ\text{C}$  and  $0.839\ \text{atm}$  with an RF power of 50 W (Figure 1c).

For comparison, the electrode configuration of a blanket film and  $\alpha$ -Si/3D-Cu electrodes with 250 and 500 nm diameter nanopillars was characterized by transmission electron microscopy (TEM) and energy-dispersive X-ray (EDX) elemental mapping (Figure 2). The structures of the  $\alpha$ -Si/3D-Cu nanopillar electrodes show clearly well-developed periodic patterns consistent with the schematic in Figure 1, as shown in Figure 2a, b, and c. Each electrode contains small pores, which were expanded during sample preparation by a focused-ion-beam treatment, at the interface between the Cu formed by e-beam evaporation and the electro-forming process, described as white spots in the TEM results. In Figure 2d, e, and f, the thickness of the  $\alpha$ -Si deposition layer was fixed at 200 nm for the blanket film and 130 nm for both  $\alpha$ -Si/3D-Cu nanopillar electrodes, and the amorphous Si structure was confirmed *via* fast Fourier transform (FFT) analysis. The thickness difference caused by  $\alpha$ -Si deposition *via* LPCVD is not relevant in this work, especially for the electrochemical test. From the energy-dispersive X-ray elemental mapping images shown in Figure 2g, h, and i, it was confirmed that the electrode structures spatially correspond to  $\alpha$ -Si and Cu and the likelihood of producing Cu silicide during processing and X-ray diffraction (XRD) analysis is low (Figure S3).<sup>37</sup>

For electrochemical characterization, the blanket film and  $\alpha$ -Si/3D-Cu nanopillar electrodes with 250 and 500 nm diameters were cycled at  $0.5\ \text{C}$  rate between 0.005 and  $1.5\ \text{V}$  in Li half-cells (2032R,  $1\ \text{C} = 2000\ \text{mA/g}$ ). The first cycle voltage profiles of each electrode are shown in Figure 3a; all electrodes exhibit no plateau below  $0.1\ \text{V}$  after lithiation, which is the typical  $\alpha$ -Si electrochemical behavior. The discharge capacities of the blanket film and  $\alpha$ -Si/3D-Cu electrodes with 250 and 500 nm diameter nanopillars during the first cycle are 1947, 1982, and 1847 mAh/g with coulomb efficiencies (C.E.) of 92.2%, 95.3%, and 91.3%, respectively.

Figure 3b exhibits the cycle retention of each electrode at  $0.5\ \text{C}$  rate. After 100 cycles, the  $\alpha$ -Si/3D-Cu electrodes with 250 and 500 nm diameter nanopillars show 1627 and 1420 mAh/g discharge capacities, respectively; on the contrary, the blanket film shows a 138 mAh/g discharge capacity with 7.1% retention.



**Figure 2.** Cross-sectional TEM images of the overall configuration of the (a) blanket film and (b and c)  $\alpha$ -Si/3D-Cu electrode with 250 and 500 nm diameter nanopillars, respectively. (d, e, and f) Expanded views of each structure at the interface between the Cu and  $\alpha$ -Si layer, as indicated in rectangular regions in a, b, and c (inset: FFT analysis for  $\alpha$ -Si). (g, h, and i) Energy-dispersive X-ray elemental mapping images of each electrode.

The main reason for the better cycle retention of the  $\alpha$ -Si/3D-Cu nanopillar electrodes is the morphology variation in each electrode before and after 100 cycles. As shown in Figure 4a and d, after 100 cycles, the blanket film electrode shows a high concentration of cracks and delamination, which is related to the strain caused by the significant mechanical stress due to the  $\alpha$ -Si volume change, resulting in a loss of electrical connectivity. In contrast, both  $\alpha$ -Si/3D-Cu nanopillar electrodes exhibited smooth surfaces even after 100 cycles (Figure 4b, c, e, and f). From Figure S4, it becomes evident that the adhesion between  $\alpha$ -Si and the Cu layer is still strong after 100 charge and discharge cycles.

These results indicate that not only do  $\alpha$ -Si 3D-nanopillar electrodes have sufficient void space to accommodate volume changes during the electrochemical reaction, but the well-patterned nanopillar substrate also allows significant enhancement of the connection between the current collector and active materials without binder. The high performance of the electrodes was confirmed by dQ/dV analysis, as shown in Figure S5. The differential plot of the first cycle exhibits two peaks at 0.08 and 0.23 V for lithiation and 0.3 and 0.48 V for delithiation.<sup>38</sup> The reversibility

was maintained without additional polarization even after 100 cycles. The retention results indicate that the electrode with a 500 nm diameter nanopillar array exhibited poorer performance than the electrode with a 250 nm diameter nanopillar array, because the free space between the nanopillars was insufficient to completely accommodate the expansion of Si, resulting in the slight deformation of the nanopillar array, as shown in the inset of Figure 4f. Also, the improved first C.E. and cycle retention of the 250 nm diameter sample compared to the 500 nm one are related to the nanopillar's resistance after volume expansion of  $\alpha$ -Si. It is reported that the resistance is increased as copper strain is developed after deformation.<sup>40</sup> Therefore, the more deformed 500 nm sample may be expected to build up a resistance, resulting in a decrease of electron transport for the charger-transfer reaction. In addition, the structural discontinuity of the deposited film plays a key role of improving the electrochemical performance of the  $\alpha$ -Si/3D-Cu nanopillar electrode. Not only can the discontinuity of the electrode provide a greater interface region between active materials and the electrolyte, but also the region where cracks exist could buffer to some degree the volume expansion (Figure S6).

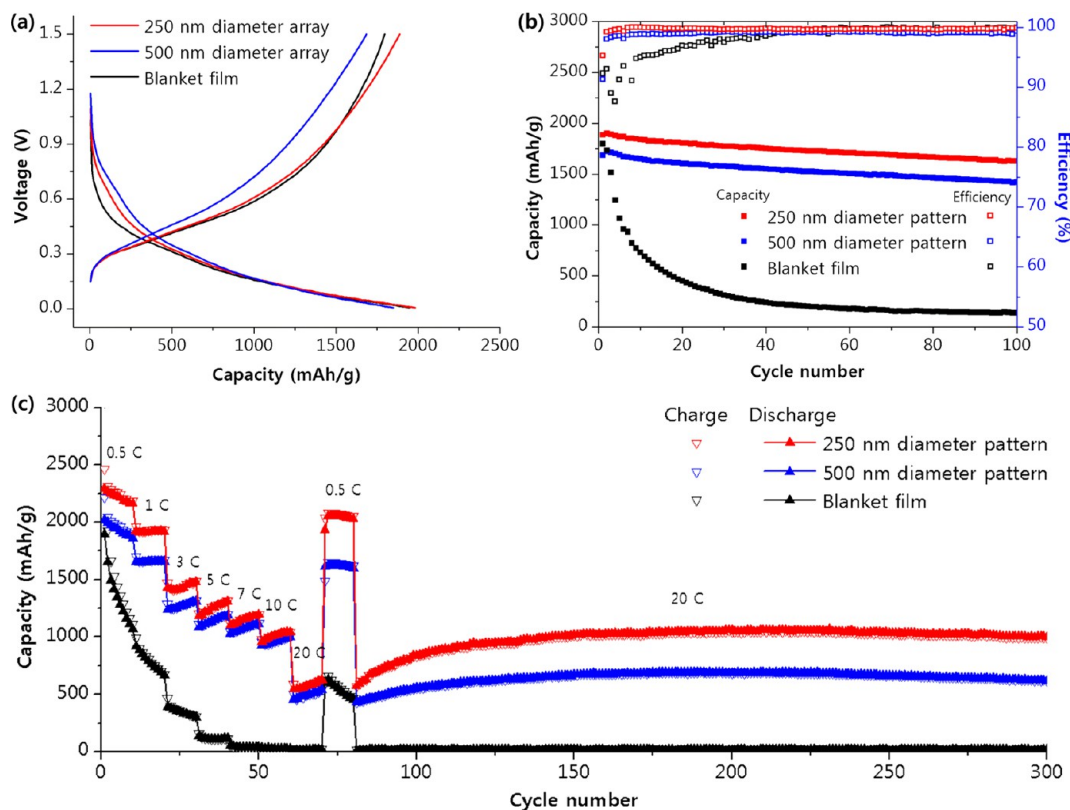


**Figure 3.** Electrochemical evaluation of 3D amorphous Si on a nanopillar Cu electrode. (a) First cycle voltage profiles of the blanket film and  $\alpha$ -Si/3D-Cu electrodes with 250 and 500 nm diameter nanopillars at 0.5 C rate. (b) Plot of the discharge capacity as a function of cycle number and coulomb efficiency at 0.5 C rate between 0.005 and 1.5 V in a 2032 coin-type half-cell (1 C = 2000 mA/g). (c) Rate capability of the blanket film and  $\alpha$ -Si/3D-Cu nanopillar electrodes with 250 and 500 nm diameter from 0.5 to 20 C rate between 0.005 and 1.5 V followed by recovery at 0.5 C, and the cycle retention plot at 20 C, respectively (the charge and discharge rates were the same).

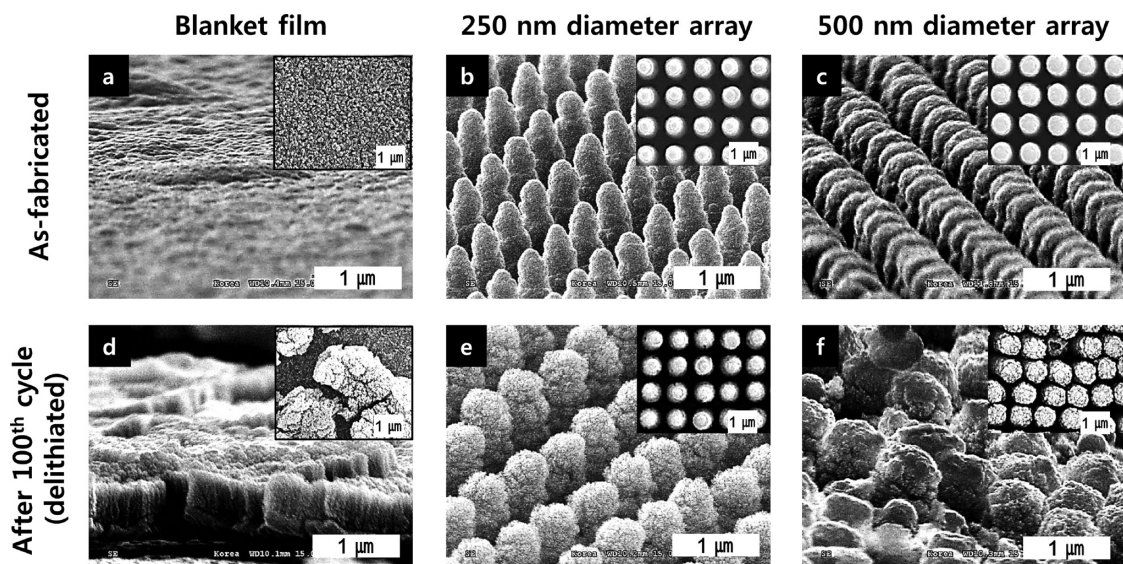


**Figure 4.** SEM images of the as-fabricated blanket film and  $\alpha$ -Si/3D-Cu electrode with 250 and 500 nm diameter nanopillars before (a, b, and c) and after 100 cycles (d, e, and f), respectively (inset: top view).

Figure 3c demonstrates the improved rate capability of both  $\alpha$ -Si/3D-Cu nanopillar electrodes from 0.5 to 20 C and improved cycle stability, even after the rate test at 20 C rate, compared to those of the blanket film electrode under the same charge and discharge

conditions (1 C = 2000 mA/g). The voltage profiles for each electrode are shown in Figure S7. The  $\alpha$ -Si/3D-Cu electrode with 250 nm diameter nanopillars exhibits discharge capacities of 2466, 1474, 1122, and 587 mAh/g at rates of 0.5, 3, 7, and 20 C, respectively, with a capacity

retention of 23.8% at 20 C; in comparison, the blanket film electrode has a capacity retention of ~0% under the same conditions. Remarkably, after the same rate test, the  $\alpha$ -Si/3D-Cu nanopillar with both 250 and 500 nm diameter electrodes underwent little capacity fading after 300 cycles at 20 C rate, showing 996 and 719 mAh/g discharging capacities with 99.3 ( $\pm 0.3$ ) and 99.9 ( $\pm 0.3$ ) % C.E., respectively. This result is comparable to that of an electrode that is surface-treated with carbon or  $\text{Al}_2\text{O}_3$ .<sup>39</sup> The capacity increase at the beginning condition in the range from 3 to 20 C may be related to the activation of the unreacted inside region of silicon, which is generally known from Si electrodes operated at high C-rate condition.<sup>41–43</sup> The maintenance of the morphology of the  $\alpha$ -Si/3D-Cu nanopillar electrodes after cycling (Figure S8) is the likely cause of the excellent cycling stability and rate performance.

## CONCLUSION

We have designed an  $\alpha$ -Si/3D-Cu nanopillar electrode resulting in improved cycle stability and rate performance, even at 20 C rate, over those of conventional planar thin-film electrodes. These excellent performances are attributed to the following reasons: First, the deposited  $\alpha$ -Si maintains good attachment to the nanopillar Cu electrode with no peeling-off due

to the 3D concavo-convex structure, which expands the contact area, and therefore it is expected to improve the rate capability. Furthermore, this unique 3D nanostructure enhances the adhesion of the  $\alpha$ -Si layer, leading to increased endurance of the  $\alpha$ -Si layer against the repeated volume change. Second, the  $\alpha$ -Si structure would be an essentially beneficial factor for the improved electrochemical behavior due to the homogeneous volume expansion/contraction with no appearance of two-phase regions unlike the crystalline structure. After 100 cycles, the thickness of the delithiated  $\alpha$ -Si layer is 190 nm, which expanded 46% from the initial thickness. Also, the amorphous phase of Si is well known to have higher diffusivity than the crystalline phase due to grain boundary characteristics, whose feature is generally a high concentration of diffusion-mediating defects due to incomplete bonding or disorder.

On the basis of these results, nanopattern technology can play a key role in enhancing the performance of various types of active materials because of the low internal resistance caused by enhanced attachment between the patterned current collector and active materials, facile charge transport due to the three-dimensional configuration, and stress relaxation as a result of the voids between the nanopillars.

## EXPERIMENTAL SECTION

**Fabrication of the  $\alpha$ -Si/3D-Cu Electrode.** The pitches and heights of the Ni metal plate stamps were 1 and 2  $\mu\text{m}$ , respectively, and the diameters of the pillars were either 250 or 500 nm. The nanoscale surface protrusion pattern of a rolled Ni metal plate stamp was transferred to polyvinyl chloride by thermal roll-to-roll processing (order production, CMP Co., Ltd.) at 100 °C under ~10 atm of pressure. Cu metal was then deposited over the embossed PVC film using e-beam evaporation at 60 °C and  $2.7 \times 10^{-5}$  atm with a rate of 3  $\text{\AA/s}$  to form a seed layer of 100 nm for the electroforming process (EBX-1000, ULVAC Inc.). Electroformation at 0.02 A for 1 h in a Cu plating solution ( $\text{CuSO}_4 \cdot 5\text{H}_2\text{O}/\text{H}_2\text{SO}_4 = 2.5:1$  with 70 ppm HCl; Americhem, Inc.) filled the cavities with Cu and formed the Cu film. Then, the Cu foil with an array of Cu nanopillars was detached from the polymer film and covered with an amorphous Si layer using LPCVD with 2%  $\text{SiH}_4$  at 200 °C and 0.839 atm under 50 W of RF power (SJF-1000T2, Sungjin Semitech Co., Ltd.).

**Fabrication of the Li-Ion Half-Cell.** A coin-shaped half-cell (2032R) was fabricated with an  $\alpha$ -Si/3D-Cu working electrode (the blanket film contains 0.136 mg of Si, corresponding to 0.088 mg/cm<sup>2</sup>, while the  $\alpha$ -Si/3D-Cu electrodes with 250 and 500 nm diameter nanopillars contain 0.142 and 0.129 mg of Si, corresponding to 0.092 and 0.084 mg/cm<sup>2</sup>, respectively) and metallic Li reference electrode. The working and reference electrode were punched for the 2032R half-cell with diameters of 14 mm and separated with a polypropylene separator. The electrolyte (Panax Korea) was 1.3 M  $\text{LiPF}_6$  in a blend of ethylene carbonate and ethyl methyl carbonate with 10 wt % flouoroethylene carbonate additive.

**Electrochemical Characterization of the Half-Cell.** For the electrochemical characterizations, the blanket film and  $\alpha$ -Si/3D-Cu electrodes with 250 and 500 nm diameter nanopillars were

cycled between 0.005 and 1.5 V in Li half-cells (2032R, 1 C = 2000 mA/g, Wonatech Co., Ltd.) at 24 °C.

**Morphology Characterization of the  $\alpha$ -Si/3D-Cu Nanopillar Electrodes.** The electrode configurations of the blanket film and  $\alpha$ -Si/3D-Cu electrodes with 250 and 500 nm diameter nanopillars were characterized by high-resolution transmission electron microscopy (JEM-2100F, JEOL Inc.), energy-dispersive spectroscopy (JEM-2100, JEOL Inc.) elemental mapping, and field emission SEM (EX-200, Horiba Inc.). The TEM sample was fabricated using a focused-ion-beam instrument (Quanta 3D FEG, FEI Inc.). The presence of  $\alpha$ -Si was confirmed via fast Fourier transform (JEM-2100, JEOL Inc.) analysis, and the crystallization of Cu was confirmed by X-ray diffraction (Rigaku) analysis.

**Conflict of Interest:** The authors declare no competing financial interest.

**Acknowledgment.** This research was supported by the Pioneer Research Center Program through the National Research Foundation of Korea funded by the Ministry of Science, ICT & Future Planning (NRF-2013M3C1A3063597), by Nano•Material Technology Development Program through the National Research Foundation of Korea (NRF) funded by the Ministry of Education, Science and Technology (2012M3A7B4035323), and by Basic Science Research Program through the National Research Foundation of Korea funded by the Ministry of Education, Science and Technology (NRF-2012-0002363). Also, the Converging Research Center Program through the Ministry of Science, ICT, and Future Planning, Korea (2013K000210), is greatly acknowledged.

**Supporting Information Available:** Additional data associated with this article are included: XRD patterns of the blanket film; differential capacity and voltage profile of the anodes; SEM and TEM images after 300 and 100 cycles. The information is available free of charge via the Internet at <http://pubs.acs.org>.

## REFERENCES AND NOTES

- Tarascon, J. M.; Armand, M. Issues and Challenges Facing Rechargeable Lithium Batteries. *Nature* **2001**, *414*, 359–367.
- Wang, J. Z.; Zhong, C.; Chou, S. L.; Liu, H. K. Flexible Free-Standing Graphene-Silicon Composite Film for Lithium-Ion Batteries. *Electrochem. Commun.* **2008**, *10*, 1913–1942.
- Chiang, Y. M. Building a Better Battery. *Science* **2010**, *330*, 1485–1486.
- Choi, N. S.; Chen, Z.; Freunberger, S. A.; Ji, X.; Sun, Y. K.; Amine, K.; Yushin, G.; Linda, F. N.; Cho, J.; Peter, G. B. Challenges Facing Lithium Batteries and Electrical Double-Layer Capacitors. *Angew. Chem., Int. Ed.* **2012**, *51*, 9994–10024.
- Nazri, G.-A.; Pistoia, G. *Lithium Batteries: Science and Technology*; Kluwer Academic/Plenum: Boston, 2004; pp 120–125.
- Huggins, R. A. Lithium Alloy Negative Electrodes. *J. Power Sources* **1999**, *81*, 13–19.
- Munao, D.; Valvo, M.; van Erven, J.; Kelder, E. M.; Hassoun, J.; Panero, S. Silicon-Based Nanocomposite for Advanced Thin Film Anodes in Lithium-Ion Batteries. *J. Mater. Chem.* **2012**, *22*, 1556–1561.
- Lee, S. W.; McDowell, M. T.; Choi, J. W.; Cui, Y. Anomalous Shape Changes of Silicon Nanopillars by Electrochemical Lithiation. *Nano Lett.* **2011**, *11*, 3034–3039.
- Liu, X. H.; Zhang, L. Q.; Zhong, L.; Liu, Y.; Zheng, H.; Wang, J. W.; Cho, J. H.; Dayeh, S. A.; Picraux, S. T.; Sullivan, J. P.; et al. Ultrafast Electrochemical Lithiation of Individual Si Nanowire Anodes. *Nano Lett.* **2011**, *11*, 2251–2258.
- Liu, X. H.; Zheng, H.; Zhong, L.; Huang, S.; Karki, K.; Zhang, L. Q.; Liu, Y.; Kushima, A.; Liang, W. T.; Wang, J. W.; et al. Anisotropic Swelling and Fracture of Silicon Nanowires during Lithiation. *Nano Lett.* **2011**, *11*, 3312–3318.
- Liu, X. H.; Zhong, L.; Huang, S.; Mao, S. X.; Zhu, T.; Huang, J. Y. Size-Dependent Fracture of Silicon Nanoparticles during Lithiation. *ACS Nano* **2012**, *6*, 1522–1531.
- Kang, B.; Ceder, G. Battery Materials for Ultrafast Charging and Discharging. *Nature* **2009**, *458*, 190–193.
- Chan, C. K.; Peng, H. L.; Liu, G.; McIlwrath, K.; Zhang, X. F.; Huggins, R. A.; Cui, Y. High-Performance Lithium Battery Anodes Using Silicon Nanowires. *Nat. Nanotechnol.* **2008**, *3*, 31–35.
- Cui, L. F.; Yang, Y.; Hsu, C. M.; Cui, Y. Carbon-Silicon Core-Shell Nanowires as High Capacity Electrode for Lithium Ion Batteries. *Nano Lett.* **2009**, *9*, 3370–3374.
- Deng, J.; Ji, H.; Yan, C.; Zhang, J.; Si, W.; Baunack, S.; Oswald, S.; Mei, Y.; Schmidt, O. G. Naturally Rolled-Up C/Si/C Trilayer Nanomembranes as Stable Anodes for Lithium-Ion Batteries with Remarkable Cycling Performance. *Angew. Chem., Int. Ed.* **2013**, *52*, 2326–2330.
- Kim, H.; Han, B.; Choo, J.; Cho, J. Three-Dimensional Porous Silicon Particles for Use in High-Performance Lithium Secondary Batteries. *Angew. Chem., Int. Ed.* **2008**, *47*, 10151–10154.
- Kim, H.; Seo, M.; Park, M. H.; Cho, J. A Critical Size of Silicon Nano-Anodes for Lithium Rechargeable Batteries. *Angew. Chem., Int. Ed.* **2010**, *49*, 2146–2149.
- Liu, N.; Wu, H.; McDowell, M. T.; Yao, Y.; Wang, C.; Cui, Y. A Yolk-Shell Design for Stabilized and Scalable Li-Ion Battery Alloy Anodes. *Nano Lett.* **2012**, *12*, 3315–3321.
- Magasinski, A.; Dixon, P.; Hertzberg, B.; Kvit, A.; Ayala, J.; Yushin, G. High-Performance Lithium-Ion Anodes Using a Hierarchical Bottom-Up Approach. *Nat. Mater.* **2010**, *9*, 353–358.
- Park, M. H.; Kim, M. G.; Joo, J.; Kim, K.; Kim, J.; Ahn, S.; Cui, Y.; Cho, J. Silicon Nanotube Battery Anodes. *Nano Lett.* **2009**, *9*, 3844–3847.
- Uday, K.; Chunsheng, W.; John, A. A. Nano- and Bulk-Silicon-Based Insertion Anodes for Lithium-Ion Secondary Cells. *J. Power Sources* **2007**, *163*, 1003–1039.
- Hong, L.; Zhaoxiang, W.; Liqian, C.; Xuejie, H. Research on Advanced Materials for Li-Ion Batteries. *Adv. Mater.* **2009**, *21*, 4593–4607.
- Dominique, L.; Shane, B.; Mathieu, M.; Kristina, E.; Jean-Claude, J.; Jean-Marie, T. Recent Findings and Prospects in the Field of Pure Metals as Negative Electrodes for Li-Ion Batteries. *J. Mater. Chem.* **2007**, *17*, 3759–3772.
- Wu, H.; Zheng, G.; Liu, N.; Carney, T. J.; Yang, Y.; Cui, Y. Engineering Empty Space between Si Nanoparticles for Lithium-Ion Battery Anodes. *Nano Lett.* **2012**, *12*, 904–909.
- Hong, L.; Xuejie, H.; Liqian, C.; Zhengang, W.; Yong, L. A High Capacity Nano-Si Composite Anode Material for Lithium Rechargeable Batteries. *Electrochem. Solid-State Lett.* **1999**, *2*, 547–549.
- Hong, L.; Xuejie, H.; Liqian, C.; Guangwen, Z.; Ze, Z.; Dapeng, Y.; Yu, J. M.; Ning, P. The Crystal Structural Evolution of Nano-Si Anode Caused by Lithium Insertion and Extraction at Room Temperature. *Solid State Ionics* **2000**, *135*, 181–191.
- Shu-Lei, C.; Jia-Zhao, W.; Mohammad, C.; Hua-Kun, L.; John, A. S.; Shi-Xue, D. Enhanced Reversible Lithium Storage in a Nanosize Silicon/Graphene Composite. *Electrochem. Commun.* **2010**, *12*, 303–306.
- Kuiqing, P.; Jiansheng, J.; Wenjun, Z.; Shuit-Tong, L. Silicon Nanowires for Rechargeable Lithium-Ion Battery Anodes. *Appl. Phys. Lett.* **2008**, *93*, 033105.
- Benjamin, H.; Alexander, A.; Gleb, Y. Deformations in Si-Li Anodes upon Electrochemical Alloying in Nano-Confining Space. *J. Am. Chem. Soc.* **2010**, *132*, 8548–8549.
- Takamura, T.; Ohara, S.; Uehara, M.; Suzuki, J.; Sekine, K. A. Vacuum Deposited Si Film Having a Li Extraction Capacity over 2000 mAh/g with a Long Cycle Life. *J. Power Sources* **2004**, *129*, 96–100.
- Maranchi, J. P.; Hepp, A. F.; Kumta, P. N. High Capacity, Reversible Silicon Thin-Film Anodes for Lithium-Ion Batteries. *Electrochem. Solid-State Lett.* **2003**, *6*, A198–A201.
- Yu, C.; Li, X.; Ma, T.; Rong, J.; Zhang, R.; Shaffer, J.; An, Y.; Liu, Q.; Wei, B.; Jiang, H. Silicon Thin Films as Anodes for High-Performance Lithium-Ion Batteries with Effective Stress Relaxation. *Adv. Energy Mater.* **2012**, *2*, 68–73.
- Nam, S. H.; Kim, K. S.; Shim, H.-S.; Lee, S. H.; Jung, G. Y.; Kim, W. B. Probing the Lithium Ion Storage Properties of Positively and Negatively Carved Silicon. *Nano Lett.* **2011**, *11*, 3656–3662.
- Gowda, S. R.; Reddy, A. L. M.; Zhan, X.; Jafry, H. R.; Ajayan, P. M. 3D Nanoporous Nanowire Current Collectors for Thin Film Microbatteries. *Nano Lett.* **2012**, *12*, 1198–1202.
- He, Y.; Yu, X.; Wang, Y.; Li, H.; Huang, X. Alumina-Coated Patterned Amorphous Silicon as the Anode for a Lithium-Ion Battery with High Coulombic Efficiency. *Adv. Mater.* **2011**, *23*, 4938–4941.
- Szczech, J. R.; Song, J. Nanostructured Silicon for High Capacity Lithium Battery Anodes. *Energy Environ. Sci.* **2011**, *4*, 56–72.
- Cho, J.-H.; Li, X.; Picraux, S. T. The Effect of Metal Silicide Formation on Silicon Nanowire-Based Lithium-Ion Battery Anode Capacity. *J. Power Sources* **2012**, *205*, 467–473.
- Pollak, E.; Salitra, G.; Baranchugov, V.; Aurbach, D. *In Situ* Conductivity, Impedance Spectroscopy, and *ex Situ* Raman Spectra of Amorphous Silicon during the Insertion/Extraction of Lithium. *J. Phys. Chem. C* **2007**, *111*, 11437–11444.
- Cao, F.-F.; Deng, J.-W.; Xin, S.; Ji, H.-X.; Schmidt, O. G.; Wan, L.-J.; Guo, Y. G. Cu-Si Nanocable Arrays as High-Rate Anode Materials for Lithium-Ion Batteries. *Adv. Mater.* **2011**, *23*, 4415–4420.
- Charsley, P.; Robins, B. A. Electrical Resistance Changes of Cyclically Deformed Copper. *Mater. Sci. Eng.* **1974**, *14*, 189–196.
- Chang, J.; Huang, X.; Zhou, G.; Cui, S.; Hallac, P. B.; Jiang, J.; Hurley, P. T.; Chen, J. Multilayered Si Nanoparticle/Reduced Graphene Oxide Hybrid as a High-Performance Lithium-Ion Battery Anode. *Adv. Mater.* **2013**, DOI: 10.1002/adma.20130257.
- Wu, H.; Chan, G.; Choi, J. W.; Ryu, I.; Yao, Y.; McDowell, M. T.; Lee, S. W.; Jackson, A.; Yang, Y.; Hu, L.; Cui, Y. Stable Cycling of Double-Walled Silicon Nanotube Battery Anodes through Solid-Electrolyte Interphase Control. *Nat. Nanotechnol.* **2012**, *7*, 310–315.
- Nguyen, H. T.; Yao, F.; Zamfir, M. R.; Biswas, C.; So, K. P.; Lee, Y. H.; Kim, S. M.; Cha, S. N.; Kim, J. M.; Pribat, D. Highly Interconnected Si Nanowires for Improved Stability Li-Ion Battery Anodes. *Adv. Energy Mater.* **2011**, *1*, 1154–1161.